The 6th International Conference on
Structural Health Monitoring of Intelligent Infrastructure
Hong Kong | 9-11 December 2013

VARIATION OF MODAL PARAMETERS OF CANTON TOWER UNDER DIFFERENT EARTHQUAKE EXCITATIONS

Yi-Cheng Liu[1], Tzung-Han Wu[2], Chin-Hsiung Loh[2] and Yi-Qing Ni[3]
[1] Dept. of Civil and Environmental Engineering, Univ. of Costa Rica, San Jose, Costa Rica.
[2] Department of Civil Engineering, National Taiwan University, Taipei 10617, Taiwan.
Email: lohc0220@ccms.ntu.edu.tw
[3] Department of Civil and Environmental Engineering, The Hong Kong Polytechnic University, China.

ABSTRACT

Earthquake source mechanism, source-site distance and magnitude may influence the structural response significantly. Among them the earthquake source-site distance is one of the interesting issues to be discussed if the vibration frequencies of the engineering structure covered a wide spectrum from very low dominant frequency to high frequency. Generally long period seismic waves can propagate much longer distance than short period waves. Therefore, for structure designed with very low fundamental frequency the effect of seismic source-distance may influence the responses of the structure. The Canton Tower located in Guangzhou, China, assures the super tall structure with fundamental frequency around 0.09 Hz. During the operation of the tower, several earthquake events had triggered the monitoring system of the structure. This paper presents the modal parameter identification of the tower. Data collected before, during, and after the seismic event are used for the identification. Three seismic event data include, Burma earthquake (long distance), Pingtong earthquake (medium distance) and Heyuan earthquake (short distance), are selected to extract the modal parameters of the tower by using SSI-COV algorithm (covariance-driven stochastic subspace identification). Data collected before, during, and after the three seismic events are used for identification. Comparison on the identified modal frequencies among these three events is discussed. It is observed that the identified modal frequencies did not change much except the results from Heyuan earthquake. The lower modal frequencies (below 1.0 Hz) did not appear for this near-site earthquake event. Finally, based on the identified system matrix (**A**) from each of the seismic event, the earthquake input force from the ground surface are estimated using recursive least square Kalman filter (RLS-KF) technique. Discussion among the identified input force from these three seismic events to the structure is made.

KEYWORDS

Stochastic Stochastic subspace identification, subspace Identification, input force identification, structural dynamics.

INTRODUCTION

In output-only characterization, the ambient response of a structure is recorded during ambient influence (i.e. without artificial excitation) by means of highly-sensitive velocity or acceleration sensing transducers. The extraction and analysis of features from spaced measurements provide a tool for structural health monitoring and damage detection. In recent years, time-domain analyses on measurement data are widely spread, such as: Eigensystem realization algorithm (ERA) [Juang 1956], Stochastic Subspace Identification (SSI) [Overschee *et al*. 1996; Peeters *et al*. 1999]. The SSI technique is a well known multivariate identification technique system which proved to be numerically stable, robust to noise perturbation and suitable for conducting non-stationarity of the ambient excitations [Van Overschee and De Moor, 1996; Peeters 2000a; 2001b]. Two basic branches exist for SSI: the covariance driven SSI-COV and data driven SSI-DATA. Application of SSI-COV and SSI-DATA had been studied [Bassville *et al.* 2007; Weng *et al.* 2008; Boonyapinyo *et al*. 2010].

The Canton Tower is located at Guangzhou, China. It is a super high-rise tube-in-tube structure as shown in Figure 3. Details of the structure can be found in references [Ni *et al*. 2009a; 2009b]. Twenty uni-axial accelerometers (Tokyo Sokushin AS-2000C) were employed for vibration measurements, and were installed at eight levels. Up to now there are many data has been collected from the vibration measurement system of the tower, including far-distance earthquake and near-site earthquake. In this paper, the acceleration response data of the tower before during and after the four events of earthquakes (Burma earthquake, Pingtong earthquake, Heyuan earthquake and Ya-An earthquake) were analyzed. Figure 1 shows the epicentres of these four events with respect to the location of Canton tower.

Figure 2 shows the recorded acceleration response from sensor node No.20 of these four earthquake events. Three time windows are specified for each event data, as indicated in Figure 2. The excitation (input) level before and during the earthquake must have differences. For ambient vibration level the stochastic subspace identification technique can be applied directly by using output measurement to extract system dynamic characteristics, while during earthquake level excitation, because there is no instrument on the foundation level, therefore, it is interesting to know the level of excitation during the earthquake or input force identification.

For input force identification, the Kalman filter based tracking approach has been studied and developed for identification of input excitation forces due to its accurate estimation in the consideration of measurement noise and modeling error. Chan et al. (1979) proposed a Kalman filter based tracking scheme with input estimation and used a detector to guard against automatic updating of the simple Kalman filter. Ma (1998) proposed an application of the Kalman filter to determine the impulse loads of a lumped-mass system in a numerical scheme. Liu et al. (2000) used the Kalman filter and least-squares estimator to determine the input excitations of a cantilever plate. The efficiency and robustness of a regularization scheme of the proposed algorithm using the Kalman filter and recursive least-squares were proven better than the conventional methods (Ma et al. 2003).

The objective of this study is to identify the dynamic characteristics of the Canton tower (mainly focus on identification of system natural frequencies) before and among different earthquake event from its output-only measurement. Discussion will also be made on the change of system natural frequencies before, during and after earthquake. Finally, the earthquake input motion at the base of the tower between Burma and Pingtong earthquakes is also identified.

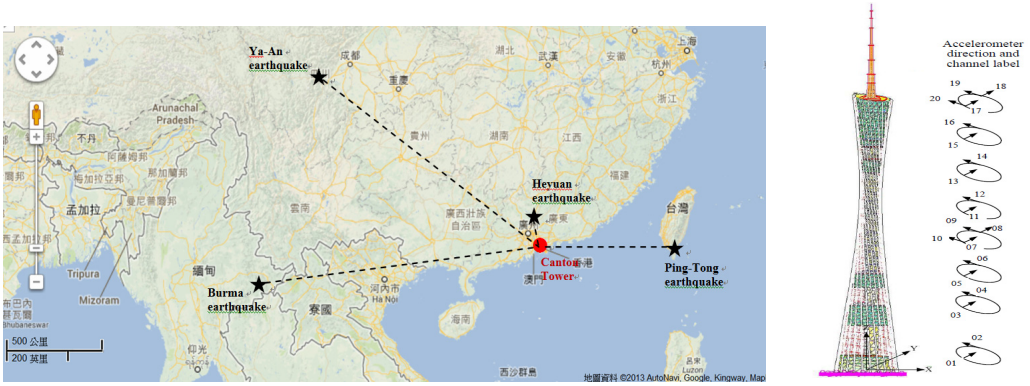

Figure 1. Epicentres of four earthquake events.

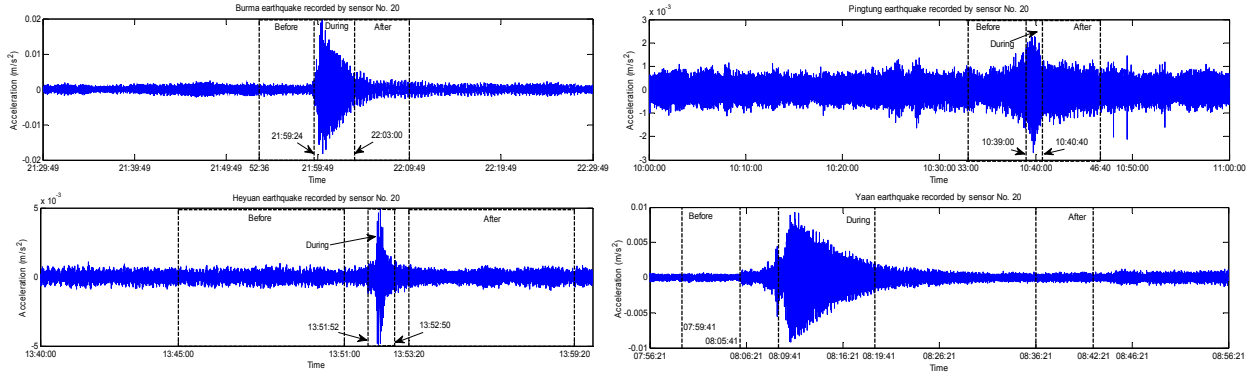

Figure 2. Acceleration response data of sensor node No.20 during the four earthquake events

METHODS OF DATA ANALYSIS

For the operational modal analysis on the tower only output measurement is analyzed. Two different approaches are used: Frequency domain decomposition (FDD) and Stochastic Subspace Identification (SSI). The Frequency Domain Decomposition (FDD) approach uses the fact that modes can be estimated from the spectral densities calculated, in the condition of a white noise input, and a lightly damped structure. It is a non-parametric technique that estimates the modal parameters directly from signal processing calculations [Brincker et al. 2000a; 2000b]. The FDD technique estimates the modes using a Singular Value Decomposition (SVD) of each of the Hermetian response spectrum matrix at each frequency and for each measurement (data set):

$$[G_{yy}(\omega)] = [V][S][V]^{H} \quad (1)$$

where $[G_{yy}(\omega)]$ is the output PSD matrix, [S] is the singular value diagonal matrix and [V] is the orthogonal matrix of the singular vectors. The singular vectors (the columns in [V]) are orthogonal to each.

To analyze the response data of Canton tower using FDD, the sampling rate of the data is 50 Hz. FDD was conducted by estimating the cross power spectral density $\boldsymbol{P_{xy}}$ of the multivariate discrete-time signals using the Welch's averaged, modified periodogram method of spectral estimation, and then, the SVD is applied to decompose the power spectral density matrix corresponding to each discrete frequency point. The largest singular value was plotted with respect to each discrete frequency. Figure 3 shows the singular spectrum of the four events data from three different time windows. It is observed that the peaks in the singular spectrum look very consistent among three events (Burma, Pingtong and Ya-An earthquakes), but the result from Heyuan earthquake looks very different from others. It indicated that the distance between the site and the epicenter may have significant effect on the response of the tower. Higher frequency modes were excited from the Heyuan earthquake because of the short epicenter distance.

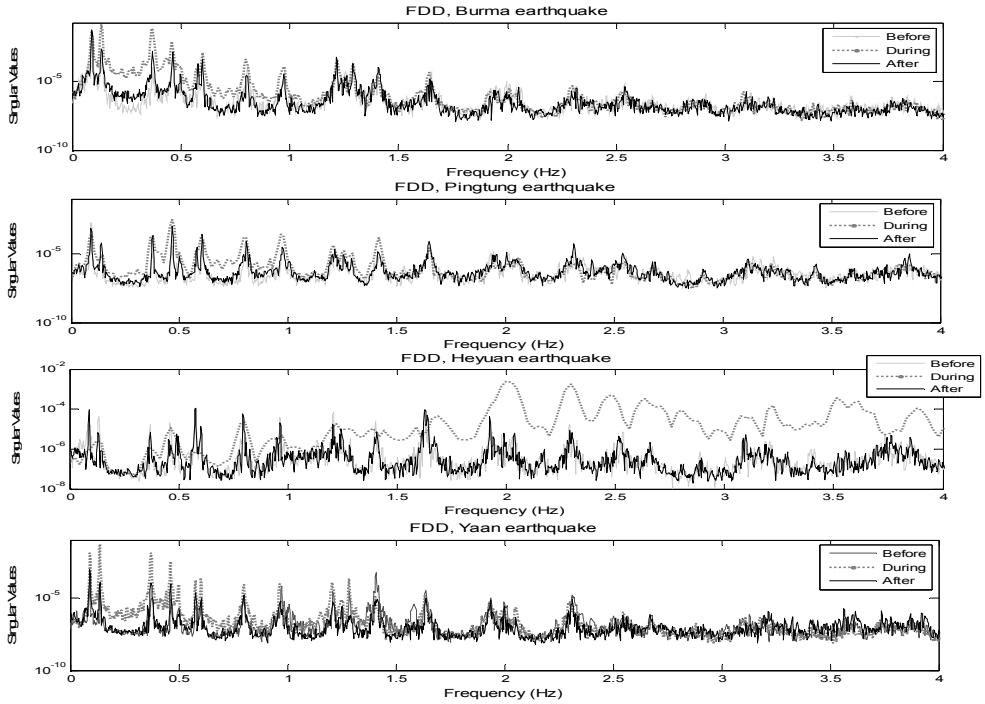

Figure 3. Plot the spectrum of singular value from FDD (from four events data)

OUTPUT-ONLY COVARIANCE-DRIVEN STOCHASTIC SUBSPACE IDENTIFICATION (SSI-COV)

To identify the system natural frequencies of the tower from its vibration measurement, the SSI-COV algorithm was used. The SSI-COV method stems from the need to solve the problem through identifying a stochastic state-space model (with matrices **A** and **C**) from output-only data. The first step is to establish the data Hankel Data matrix and then form the block Toeplitz matrix by a multiplication between future and transpose of past measurements:

$$\mathbf{H} = \frac{1}{\sqrt{\mathbf{N}}} \begin{bmatrix} \mathbf{y}_1 & \mathbf{y}_2 & \cdots & \mathbf{y}_N \\ \mathbf{y}_2 & \mathbf{y}_3 & \cdots & \mathbf{y}_{N+1} \\ \cdots & \cdots & \cdots & \cdots \\ \mathbf{y}_i & \mathbf{y}_{i+1} & \cdots & \mathbf{y}_{i+N-1} \\ \mathbf{y}_{i+1} & \mathbf{y}_{i+2} & \cdots & \mathbf{y}_{i+N} \\ \mathbf{y}_{i+2} & \mathbf{y}_{i+3} & \cdots & \mathbf{y}_{i+N+1} \\ \cdots & \cdots & \cdots & \cdots \\ \mathbf{y}_{2i} & \mathbf{y}_{2i+1} & \cdots & \mathbf{y}_{2i+N-1} \end{bmatrix} = \begin{bmatrix} \mathbf{Y_p} \\ \mathbf{Y_f} \end{bmatrix} \quad \Rightarrow \quad \boldsymbol{T}_{1/i} = \begin{bmatrix} \boldsymbol{R}_i & \boldsymbol{R}_{i-1} & \cdots & \boldsymbol{R}_1 \\ \boldsymbol{R}_{i+1} & \boldsymbol{R}_i & \cdots & \boldsymbol{R}_2 \\ \cdots & \cdots & \cdots & \cdots \\ \boldsymbol{R}_{2i-1} & \boldsymbol{R}_{2i-2} & \cdots & \boldsymbol{R}_i \end{bmatrix} = \boldsymbol{Y}_f (\boldsymbol{Y}_p)^T \quad (2)$$

where $\mathbf{Y}_p$ denotes the past measurements and $\mathbf{Y}_f$ denotes for the future measurements. The block output covariance with time lag i is defined as $\mathbf{R}_i$ and has the following factorization properties:

$$\mathbf{R}_i = \mathrm{E}[\mathbf{y}_k \, \mathbf{y}_{k-i}^T] = \mathbf{C}\mathbf{A}^{i-1}\mathbf{G} \quad (3)$$

where $\mathbf{G}$ is the next-step state and output covariance matrix $\mathbf{G} = E[\boldsymbol{x}_{k+1}\boldsymbol{y}_k^T]$. The Toeplitz matrix can be factorized into the extended observability matrix $\mathbf{O}_i \in \Re^{li\times 2n}$ and the reversed extended stochastic controllability matrix $\boldsymbol{\Gamma}_i \in \Re^{2n\times li}$, as shown below:

$$\mathbf{T}_{1/i} = \mathbf{O}_i\boldsymbol{\Gamma}_i = \begin{bmatrix} \mathbf{C} \\ \mathbf{CA} \\ \dots \\ \mathbf{CA}^{i-1} \end{bmatrix} \begin{bmatrix} \mathbf{A}^{i-1}\mathbf{G} & \dots & \mathbf{AG} & \mathbf{G} \end{bmatrix} \tag{4}$$

Singular Value Decomposition (SVD) is then applied to perform the above mentioned factorization:

$$\mathbf{T}_{1/i} = \mathbf{USV}^T = \begin{pmatrix} \mathbf{U}_1 & \mathbf{U}_2 \end{pmatrix} \begin{pmatrix} \mathbf{S}_1 & 0 \\ 0 & 0 \end{pmatrix} \begin{pmatrix} \mathbf{V}_1^T \\ \mathbf{V}_2^T \end{pmatrix} = \mathbf{U}_1\mathbf{S}_1\mathbf{V}_1^T \tag{5}$$

where $\mathbf{U} \in \Re^{li\times li}$ and $\mathbf{V} \in \Re^{li\times li}$ are orthonormal matrices, and $\mathbf{S}$ is a diagonal matrix containing positive singular values in descending order. Comparing (4) and (5), the matrix $\mathbf{O}_i$ which contains the system matrices ($\mathbf{A}$ and $\mathbf{C}$) can be computed by splitting the SVD in two parts:

$$\mathbf{O}_i = \mathbf{U}_1 \mathbf{S}_1^{1/2} \quad , \quad \boldsymbol{\Gamma}_i = \mathbf{S}_1^{1/2}\mathbf{V}_1^T \tag{6}$$

From $\mathbf{O}_i$ matrix, the system matrices ($\mathbf{A}$ and $\mathbf{C}$) can be obtained easily. In MATLAB notation, the C matrix is just the first block of $\mathbf{O}_i$, i.e. $C = O_i(1:l,:)$. Then system matrix $\mathbf{A}$ can be computed by exploiting the shift structure of the extended observability matrix $\mathbf{O}_i$:

$$\begin{bmatrix} \mathbf{CA} \\ \mathbf{CA}^2 \\ \dots \\ \mathbf{CA}^i \end{bmatrix} = \begin{bmatrix} \mathbf{C} \\ \mathbf{CA} \\ \dots \\ \mathbf{CA}^{i-1} \end{bmatrix} \mathbf{A} \quad \text{and} \quad \mathbf{A} = \mathbf{O}_i(1{:}l(i-1),:)^{\dagger}\mathbf{O}_i(l+1{:}li,:) \tag{7}$$

where $(\cdot)^{\dagger}$ denotes pseudo-inverse. The system matrix $\mathbf{A}$ is extracted by taking advantage of the shift structure of matrix $\mathbf{O}_i$, and the pseudo-inverse of $\mathbf{O}_i$ is to determine the system matrix $\mathbf{A}$ in a least square sense. The modal frequencies and effective damping ratios can be computed by conducting eigenvalue decomposition of the system matrix $\mathbf{A}$, and the corresponding eigenvectors multiplied by the output matrix $\mathbf{C}$ are used to observe mode shapes.

Application of SSI-COV to Data from Canton Tower Measurement

To analyze the data recorded from the ambient vibration as well as the earthquake excitation data of Canton tower, the SSI-COV is used. Down-sampling rate on the data was conducted (from 50 Hz to 12.5 Hz) by using low-pass filter (Butterworth IIR filter with order 10). For the analysis of each event, three different time windows are selected (as indicated in Figure 2). Length of data during earthquake is specified as follows:

- Burma earthquake: 4 min. 24 seconds data length (13200 points with 50 Hz sampling rate)
- Pingtong earthquake: 100 seconds data length (5000 points with 50 Hz sampling rate)
- Heyuan earthquake: 58 seconds data length (2900 points with 50 Hz sampling rate)

In SSI-COV the system order is fixed to 120 and the results are extracted from 90 block rows. Figure 4 shows the identified system natural frequencies and plotted with stability diagram using different system order before during and after earthquakes. It is observed that before and after the earthquakes, the tower system natural frequencies did not change much which indicated the dynamic characteristics of the tower remains the same before and after earthquakes. It is interesting to note that the identified system natural frequencies from data of Heyuan earthquake show different results. Higher system natural frequencies (>2.0 Hz) can be identified than the lower frequencies as compare to other events. This because the epicenter of Heyuan earthquake is very close to the tower location and the input excitation may contain significant higher frequency signals than other far distance earthquakes. The singular spectrum from FDD is also plot in the stability diagram. Comparison on the identified system natural frequencies (for frequency below 2.0 Hz) before all the earthquakes is very similar.. Results from Burma earthquake and Ya-An earthquake are quite similar even during the earthquake (because they are with almost the same epicenter distance).

It is noted that the measurement system of Canton tower is mainly designed for continuous structural health monitoring (not the earthquake event monitoring), therefore, there is no instrumentation was put in the basement of the tower to record the input ground motion. It is interesting to reconstruct the input motion using the response measurement. In this study the input force identification is also presented. Both Burma earthquake and Pintong earthquake data are used for discussion the input earthquake force applied on the tower structure.

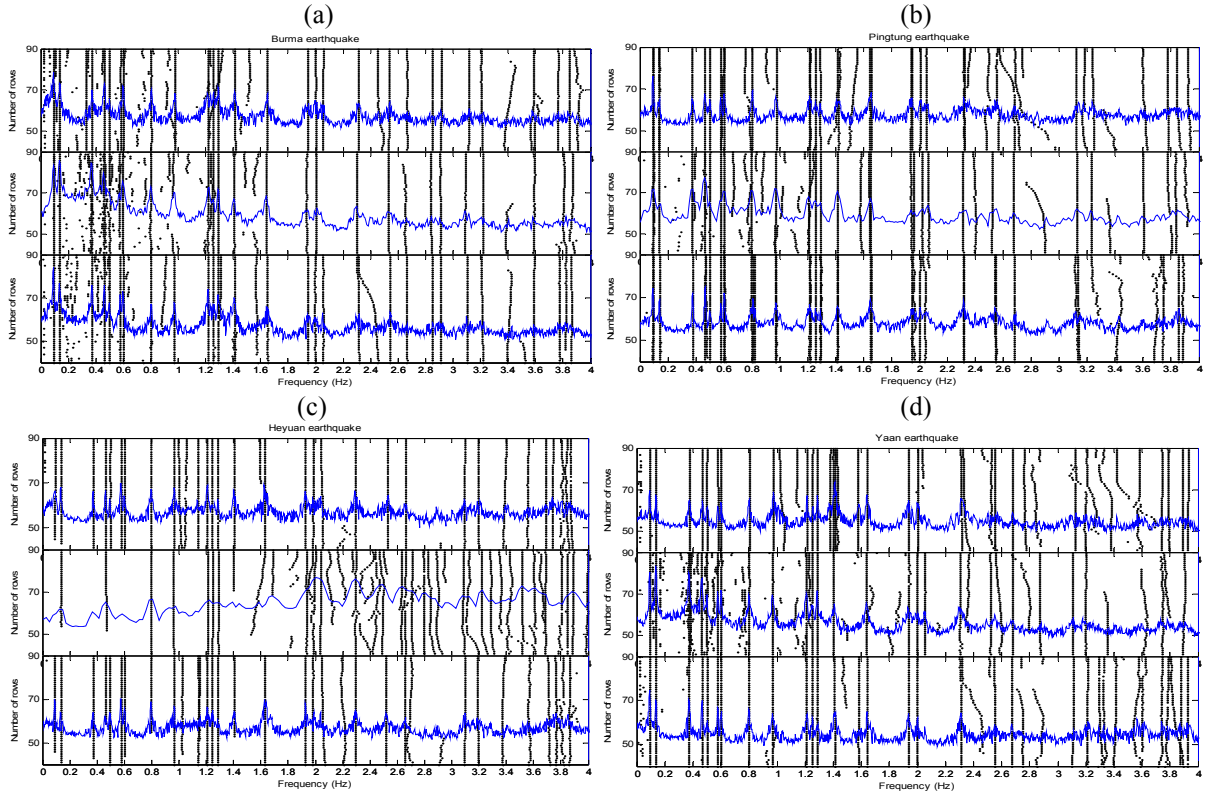

Figure 4. System frequencies plotted with stability diagram before (top) during (middle) and after (below) (a) Burma Earthquake, (b) Pingtong Earthquake, (c) Heyuan earthquake), (d) Ya-An earthquake

THEORETICAL BACKGROUND OF INPUT FORCE RECONSTRUCTION

Consider a n degree-of-freedom lumped-mass system, the equation of motion can be written as follows:

$$\mathbf{M}\ddot{\mathbf{Y}}(\mathrm{t}) + \mathbf{C}\dot{\mathbf{Y}}(\mathrm{t}) + \mathbf{K}\mathbf{Y}(\mathrm{t}) = \mathbf{F}(\mathrm{t}) \tag{8}$$

where $\mathbf{M}$ denotes the $n \times n$ mass matrix, $\mathbf{C}$ is the $n \times n$ damping matrix, $\mathbf{K}$ is the $n \times n$ stiffness matrix, $\mathbf{F}(\mathrm{t})$ is the $n \times 1$ input force vector, $\ddot{\mathbf{Y}}(\mathrm{t})$, $\dot{\mathbf{Y}}(\mathrm{t})$ and $\mathbf{Y}(\mathrm{t})$ are $n \times 1$ vectors of acceleration, velocity and displacement, respectively. To estimate the states of linear system through the Kalman filter, the transformation of the equations of motion is performed. The dynamic system with n degrees of freedom will be represented by $2n \times 1$ state vectors: $\mathbf{X}(\mathrm{t}) = [\mathbf{Y}(\mathrm{t}) \quad \dot{\mathbf{Y}}(\mathrm{t})]$. According to Equation (8), the continuous-time state and measurement equations can be written as follows:

$$\mathbf{X(k+1)} = \mathbf{AX(k)} + \mathbf{BF(k)} + \mathbf{\Gamma w(k)} \tag{9}$$

$$\mathbf{Z(k)} = \mathbf{HX(k)} + \mathbf{v(k)} \tag{10}$$

where

$$\mathbf{X(t)} = [X_1(t) \quad X_2(t) \quad \ldots \quad X_{2n-1}(t) \quad X_{2n}(t)]^T, \tag{10a}$$

$$\mathbf{F(t)} = [F_1(t) \quad F_2(t) \quad F_3(t) \quad \cdots \quad F_n(t)]^T, \qquad \mathbf{Z(k)} = [Z_1(k) \quad Z_2(k) \quad Z_3(k) \quad \cdots \quad Z_n(k)]^T$$

Equations (9) and (10) are discrete form over time interval of length Δt, and associated with process noise involving statistical description of the system noise and uncertainty in the dynamic models. **X(k)** represents the state vector, **A** is the state transition matrix, **B** is the input matrix, Δt is the sampling interval, **F(k)** is the sequence of the deterministic input, and ***w(k)*** is the noise vector which is assumed to be zero mean and white with variance $E[w(k)w^T(j)] = Q\delta_k$, where Q is the process noise covariance matrix and δ_k is the Kronecker delta. **Z(k)** denotes the observation vector and $v(k)$ represents the measurement noise vector. In addition, $v(k)$ is assumed to be zero mean and white noise. The variance of $v(k)$ is given by $E[v(k)v^T(j)] = R\delta_k$, where R is the measurement noise covariance matrix. Procedures for the input force identification are listed as follows:

First, provides a recursive relationship between a residual innovation resulting from the Kalman filter and input excitation force. Let $\hat{\mathbf{X}}$**(k/k)** and $\overline{\mathbf{X}}$**(k/k)** respectively denote the predicted state **X(k)** with and without input excitation force, **F(k–1)**. The update state estimation without inputs can be expressed as:

$$\begin{aligned}\overline{\mathbf{X}}(\mathbf{k/k}) &= \overline{\mathbf{X}}(\mathbf{k/k-1}) + \mathbf{K}_a\overline{\mathbf{Z}}(\mathbf{k}) \\ &= [\mathbf{I} - \mathbf{HK}_a(\mathbf{k})]\,\boldsymbol{\Phi}\overline{\mathbf{X}}(\mathbf{k-1/k-1}) + \mathbf{K}_a(\mathbf{k})\mathbf{Z}(\mathbf{k})\end{aligned} \tag{11}$$

And the update state estimation with input can be expressed as:

$$\begin{aligned}\hat{\mathbf{X}}(\mathbf{k/k}) &= \hat{\mathbf{X}}(\mathbf{k/k-1}) + \mathbf{K}_a\hat{\mathbf{Z}}(\mathbf{k}) \\ &= [\mathbf{I} - \mathbf{HK}_a(\mathbf{k})][\,\boldsymbol{\Phi}\hat{\mathbf{X}}(\mathbf{k-1/k-1}) + \boldsymbol{\Gamma}\mathbf{F}] + \mathbf{K}_a(\mathbf{k})\mathbf{Z}(\mathbf{k})\end{aligned} \tag{12}$$

Second, define the difference between $\hat{\mathbf{X}}(\mathbf{k/k})$ and. $\overline{\mathbf{X}}(\mathbf{k/k})$ It is now define

$$\begin{aligned}\Delta\mathbf{X}(\mathbf{k/k}) &= \hat{\mathbf{X}}(\mathbf{k/k}) - \overline{\mathbf{X}}(\mathbf{k/k}) \\ &= [\mathbf{I} - \mathbf{HK}_a(\mathbf{k})][\boldsymbol{\Phi}\mathbf{k})][\quad -1/\mathbf{k}-1) + \boldsymbol{\Gamma}\mathbf{F}] = \mathbf{M}_s(\mathbf{k})\boldsymbol{\Gamma}\mathbf{k}\end{aligned} \tag{13}$$

where

$$= [\mathbf{I} - \mathbf{HK}_a(\mathbf{k})][\boldsymbol{\Phi}\mathbf{k}\ _s(\mathbf{k}-1) + \mathbf{I}]\boldsymbol{\Gamma}] \tag{14}$$

The relationship between the two estimations is expressed as

$$\hat{\mathbf{X}}(\mathbf{k/k}) = \overline{\mathbf{X}}(\mathbf{k/k}) + \mathbf{M}_s(\mathbf{k})\boldsymbol{\Gamma}\mathbf{k} \tag{15}$$

where

$$\mathbf{M}_s(\mathbf{k}) = [\mathbf{I} - \mathbf{K}_a(\mathbf{k})\mathbf{H}][\,\boldsymbol{\Phi}\mathbf{k}\ _s(\mathbf{k}-1) + \mathbf{I}]$$

Third, let $\hat{\mathbf{Z}}(\mathbf{k})$ and $\overline{\mathbf{Z}}(\mathbf{k})$ denote the innovation $\mathbf{Z}(\mathbf{k})$ with and without input excitation forces $\mathbf{F}(\mathbf{k}-\mathbf{1})$, respectively. The difference between $\hat{\mathbf{Z}}(\mathbf{k})$ and $\overline{\mathbf{Z}}(\mathbf{k})$ can be expressed as

$$\begin{aligned}\overline{\mathbf{Z}}(\mathbf{k}) - \hat{\mathbf{Z}}(\mathbf{k}) &= \mathbf{H}\boldsymbol{\Phi}\hat{\mathbf{X}}(\mathbf{k}-\mathbf{1/k}-\mathbf{1}) - \mathbf{H}\boldsymbol{\Phi}\overline{\mathbf{X}}(\mathbf{k}-\mathbf{1/k}-\mathbf{1}) + \mathbf{H}\boldsymbol{\Gamma}\boldsymbol{\Gamma} \\ &= \mathbf{H}[\,\boldsymbol{\Phi}[\quad _s(\mathbf{k}-\mathbf{1}) + \mathbf{I}]\,\boldsymbol{\Gamma}]\end{aligned} \tag{16}$$

Therefore the difference between $\hat{\mathbf{Z}}(\mathbf{k})$ and $\overline{\mathbf{Z}}(\mathbf{k})$ can be expressed as

$$\overline{\mathbf{Z}}(\mathbf{k}) = \mathbf{Z}(\mathbf{k}) + \mathbf{B}_S(\mathbf{k})\mathbf{F} \qquad \text{with} \qquad \mathbf{B}_S = \mathbf{H}(\boldsymbol{\Phi}\,\mathbf{M}_S(\mathbf{k}-\mathbf{1}) + \mathbf{I})\boldsymbol{\Gamma} \tag{17}$$

Now considering time step $k = m, m+1, \cdots m+n$, Equation (17) can be rewritten as:

$$\Re(\mathbf{N}) = \mathbf{B}_s(\mathbf{N})\mathbf{F} + \boldsymbol{\varepsilon}(\mathbf{N}) \tag{18}$$

where $\Re(\mathbf{N}) = [\overline{\mathbf{Z}}(\mathbf{m}+\mathbf{1}) \quad \overline{\mathbf{Z}}(\mathbf{m}+\mathbf{2}) \quad \ldots \quad \overline{\mathbf{Z}}(\mathbf{m}+\mathbf{n})]^{\mathrm{T}}$ and $\boldsymbol{\varepsilon}(\mathbf{N}) = [\hat{\mathbf{Z}}(\mathbf{m}+\mathbf{1}) \quad \hat{\mathbf{Z}}(\mathbf{m}+\mathbf{2}) \quad \ldots \quad \hat{\mathbf{Z}}(\mathbf{m}+\mathbf{n})]^{\mathrm{T}}$

$$\mathbf{B}_s(\mathbf{N}) = \begin{bmatrix}\mathbf{B}_s(\mathbf{m}+\mathbf{1}) \\ \mathbf{B}_s(\mathbf{m}+\mathbf{2}) \\ \vdots \\ \mathbf{B}_s(\mathbf{m}+\mathbf{n})\end{bmatrix} = \begin{bmatrix}\mathbf{H}\boldsymbol{\Gamma} \\ \mathbf{H}(\boldsymbol{\Phi}(\quad _s(\mathbf{m}+\mathbf{1})+\mathbf{I})\boldsymbol{\Gamma} \\ \vdots \\ \mathbf{H}(\boldsymbol{\Phi}(\quad _s(\mathbf{m}+\mathbf{n}-\mathbf{1})+\mathbf{I})\boldsymbol{\Gamma}\end{bmatrix} \tag{19}$$

From this equation, $\varepsilon(N)$ can be treated as a disturbance vector, whose covariance can be denoted as:

$$\boldsymbol{\Lambda}(\mathbf{N}) = \begin{bmatrix}\mathbf{S}(\mathbf{m}+\mathbf{1}) & \mathbf{0} & \cdots & \mathbf{0} \\ \mathbf{0} & \mathbf{S}(\mathbf{m}+\mathbf{2}) & \cdots & \mathbf{0} \\ \vdots & \vdots & \ddots & \vdots \\ \mathbf{0} & \mathbf{0} & \cdots & \mathbf{S}(\mathbf{m}+\mathbf{n})\end{bmatrix} \tag{20}$$

where

$$\mathbf{S}(\mathbf{k}) = \mathbf{E}[\hat{\mathbf{Z}}(\mathbf{k})\hat{\mathbf{Z}}(\mathbf{k})] = \mathbf{HP}(\mathbf{k/k}\quad -1)\mathbf{H}^{\mathrm{T}} + \mathbf{R} \tag{20a}$$

Equation (17) provides the recursive relationship between the residual innovation and the input excitation forces. Therefore, a least-squares algorithm is employed to solve the corresponding input loads and the result in a batch form can be obtained as follow (detail derivation can be seen in Wu *et al*. [2009]:

$$\hat{\mathbf{F}}(\mathbf{N}) = [\mathbf{B}_s{}^{\mathrm{T}}(\mathbf{N})\boldsymbol{\Lambda}^{-1}(\mathbf{N})\mathbf{B}_s(\mathbf{N})]^{-1}\mathbf{B}_s{}^{\mathrm{T}}(\mathbf{N})\boldsymbol{\Lambda}^{-1}(\mathbf{N})\Re(\mathbf{N}) \tag{21a}$$

And the error covariance is:

$$\mathbf{P}_b(\mathbf{N}) = \mathbf{E}[(\mathbf{F} - \hat{\mathbf{F}}(\mathbf{N}))(\mathbf{F} - \hat{\mathbf{F}}(\mathbf{N}))^{\mathrm{T}}] = [\mathbf{B}_s{}^{\mathrm{T}}(\mathbf{N})\boldsymbol{\Lambda}^{-1}(\mathbf{N})\mathbf{B}_s(\mathbf{N})]^{-1} \tag{21b}$$

Then the recursive least-squares algorithm can be derived by considering the next time step $k = m+n+1$. By applying the matrix inversion lemma and the recursive least-square technique, the input force can be identified.

To implement the input force identification technique to identify the earthquake excitation on Canton tower, the equation of motion of the tower needs to be derived:

$$\mathbf{M}\{\ddot{\mathbf{v}}\} + \mathbf{C}\{\dot{\mathbf{v}}\} + \mathbf{K}\{\mathbf{v}\} = -\mathbf{M}\{\mathbf{1}\}\ddot{v}_g(\mathrm{t}) \tag{22}$$

In terms of modal equation (define $\{\mathbf{v}\} = [\mathbf{\Phi}]\{\mathbf{y}\}$), Equation (22) can be expressed as:

$$[\overline{\mathbf{M}}]\{\ddot{\mathbf{y}}\} + [\overline{\mathbf{C}}]\{\dot{\mathbf{y}}\} + [\overline{\mathbf{K}}]\{\mathbf{y}\} = -[\mathbf{\Phi}]^{\mathrm{T}}[\mathbf{M}]\{\mathbf{1}\}\ddot{v}_g(t) \tag{23}$$

or expressed in the state space equation:

$$\begin{Bmatrix}\dot{\mathbf{y}}\\ \ddot{\mathbf{y}}\end{Bmatrix} = \begin{bmatrix}\mathbf{0} & \mathbf{I}\\ -\overline{\mathbf{M}}^{-1}\overline{\mathbf{K}} & -\overline{\mathbf{M}}^{-1}\overline{\mathbf{C}}\end{bmatrix}\begin{Bmatrix}\mathbf{y}\\ \dot{\mathbf{y}}\end{Bmatrix} - \begin{bmatrix}\mathbf{0}\\ \mathbf{I}\end{bmatrix}[\overline{\mathbf{M}}]^{-1}[\mathbf{\Phi}]^{\mathrm{T}}[\mathbf{M}]\{\mathbf{1}\}\ddot{v}_g(t) \tag{24}$$

Since $\{\mathbf{y}\} = [\mathbf{\Phi}]^{\mathrm{T}}\{\mathbf{v}\}$ and substitute into the state space equation, then

$$\begin{Bmatrix}\dot{\mathbf{v}}\\ \ddot{\mathbf{v}}\end{Bmatrix} = \begin{bmatrix}\mathbf{0} & \mathbf{I}\\ -\overline{\mathbf{M}}^{-1}\overline{\mathbf{K}} & -\overline{\mathbf{M}}^{-1}\overline{\mathbf{C}}\end{bmatrix}\begin{Bmatrix}\mathbf{v}\\ \dot{\mathbf{v}}\end{Bmatrix} - \begin{bmatrix}\mathbf{0}\\ [\mathbf{I}]\end{bmatrix}[\mathbf{\Phi}][\overline{\mathbf{M}}]^{-1}[\mathbf{\Phi}]^{\mathrm{T}}[\mathbf{M}]\{\mathbf{1}\}\ddot{v}_g(t) \tag{25}$$

or

$$\mathbf{X}_{\mathbf{k}+1} = \mathbf{A}\mathbf{X}_{\mathbf{k}} + \mathbf{B}\mathbf{F}_{\mathbf{k}} \tag{25a}$$

where $\mathbf{X}_{\mathbf{k}} = \begin{Bmatrix}\mathbf{v}\\ \dot{\mathbf{v}}\end{Bmatrix}$, $\mathbf{A} = \begin{bmatrix}\mathbf{0} & \mathbf{I}\\ -\overline{\mathbf{M}}^{-1}\overline{\mathbf{K}} & -\overline{\mathbf{M}}^{-1}\overline{\mathbf{C}}\end{bmatrix}$, $\mathbf{B} = \begin{bmatrix}\mathbf{0}\\ [\mathbf{I}]\end{bmatrix}$ and the input force can be expressed as

$$Input\ \ Force = [\mathbf{\Phi}][\overline{\mathbf{M}}]^{-1}[\mathbf{\Phi}]^{\mathrm{T}}[\mathbf{M}]\{\mathbf{1}\}\ddot{v}_g(t) = [\mathbf{\Phi}]\left\{\frac{\{\mathbf{\varphi}_i\}^{\mathrm{T}}[\mathbf{M}]\{\mathbf{1}\}}{\overline{m}_i}\right\}\ddot{v}_g(t) \tag{26}$$

Equation (25) shows the state-space equation of a system with the consideration of input which is exactly the same as Equation (9). For case of absolution acceleration response measurement (as it is from Canton tower), the measurement (or observation) equation can be expressed as:

$$\mathbf{Z}_{\mathbf{k}} = \mathbf{H}\mathbf{X}_{\mathbf{k}} \tag{27}$$

where the measurement matrix is defined as $\mathbf{H} = \begin{bmatrix}-\overline{\mathbf{M}}^{-1}\overline{\mathbf{K}} & -\overline{\mathbf{M}}^{-1}\overline{\mathbf{C}}\end{bmatrix}$. Both Equations (25) and (27) are exactly the same as the formulation for input for identification. The measurement matrix contains the normalized stiffness and normalized damping matrices. Both the normalized stiffness matrix and damping matrix can be reconstructed from the identified model characteristics (1.e. mode shapes and damping ratios) [Amani *et al.* 2007].

DISCUSSION ON INPUT FORCE OF CANTON TOWER DURING EARTHQUAKE EXCITATIONS

To identify the input force function during the earthquake excitation, it is necessary to obtain the measurement matrix, as shown in Equation (27). From the SSI-COV one can identify the system natural frequencies and damping ratios from which the normalized system stiffness and damping matrices can be determined. Then, by using the Kalman filter equations, as derived above, to obtain the innovation covariance $\mathbf{S(k)}$, innovation $\overline{\mathbf{Z}}\mathbf{(k)}$ and Kalman gain $\mathbf{K}_{\mathbf{a}}\mathbf{(k)}$. With the recursive least-squares algorithm the input forces $\hat{\mathbf{F}}\mathbf{(k)}$ can be estimated.

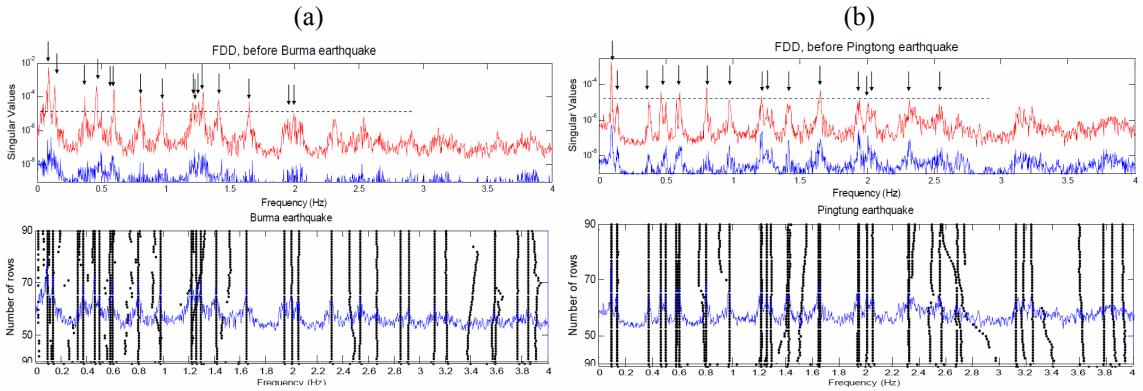

Figure 5. Comparison on the identified first 16 modes from FDD and SSI for (a) Burma earthquake and (b) Pingtong earthquakes (using ambient vibration data)

Now consider the tower as a stick model with 8 degree-of-freedom system. It is assumed that the lumped mass is assigned at each measured level; therefore, a total of 8 nodes were used. In this study, only the first 16 modes (8 modes from X-direction and the other 8 modes from Y-direction) will be used which are in consistent with the measurement degree of freedoms. Figure 5 shows the selected 16 modes to reconstruct the normalized stiffness and damping matrices. Comparison on these selected 16 modes (model frequencies) with the results from FDD and SSI is also shown in Figure 5. It is observed that the selected 16 modes from Burma earthquake are all within 2.0 Hz.

From the observation of the distribution of singular spectrum in FDD, all the selected 16 modes are the largest singular spectrum in FDD analysis, as shown in Figure (5a). From the distribution of singular spectrum in FDD analysis of Pingtong earthquake, the identified 16 modes are with frequencies larger than 2.0 Hz. Figures 6a and 7a show the identified mode shapes from the ambient data before Burma and Pingtong earthquake, respectively. With these identified mode shapes and normalized stiffness matrix can be constructed. The identified input forcing function on the tower for Burma earthquake and Pingtong earthquake are shown in Figures 6b and 7b, respectively. It is important to pointed out that the frequency content of the identified input forcing function is focus on low frequencies: for Burma earthquake <2.0 Hz; for Pingtong earthquake <5.0 Hz. This because the selected model frequencies is different for these two events.

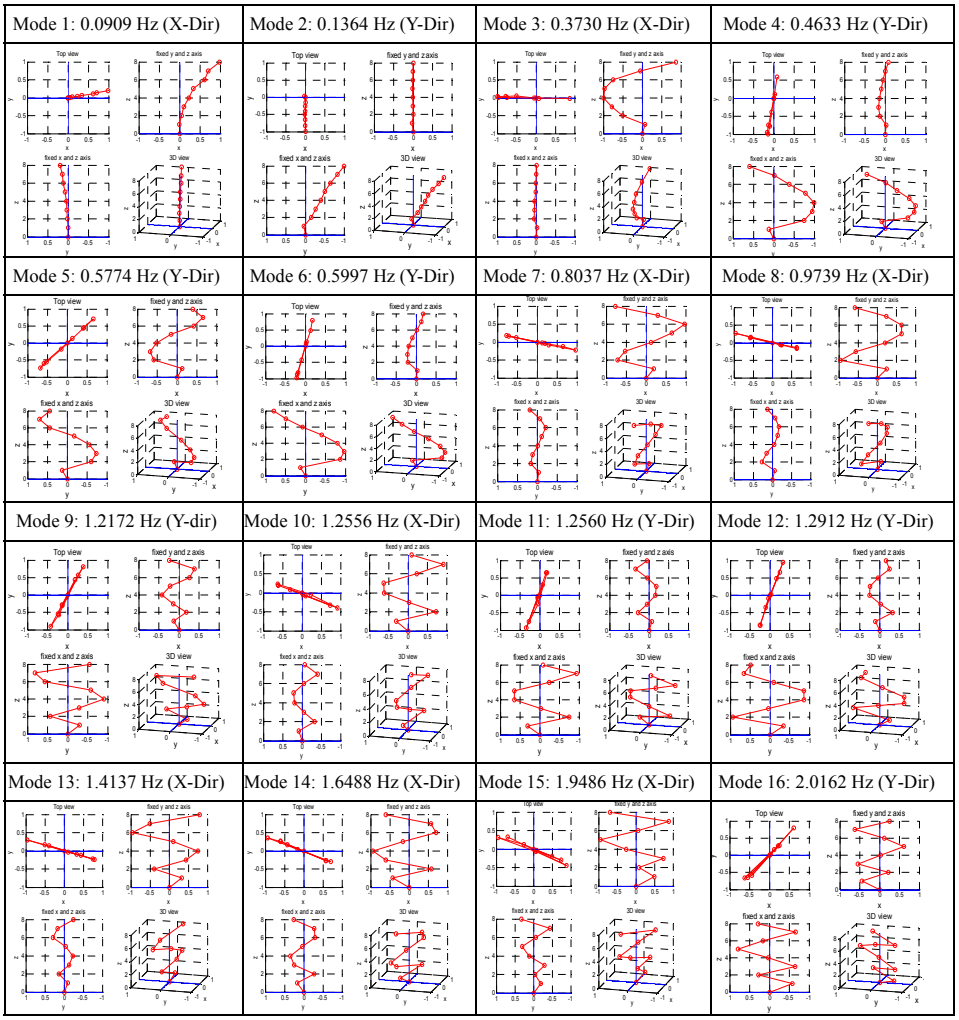

Figure 6a. Identified 16 mode shapes (top view, x- and y- direction, 3-D) from Burma earthquake

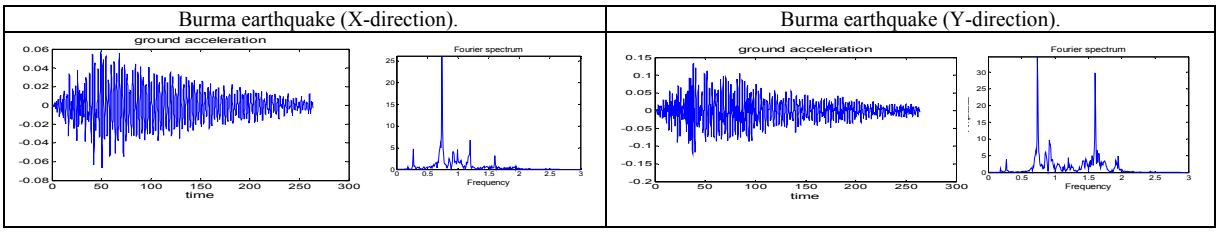

Figure 6b: Identified input forcing function on Canton tower and its Fourier amplitude (Burma earthquake).

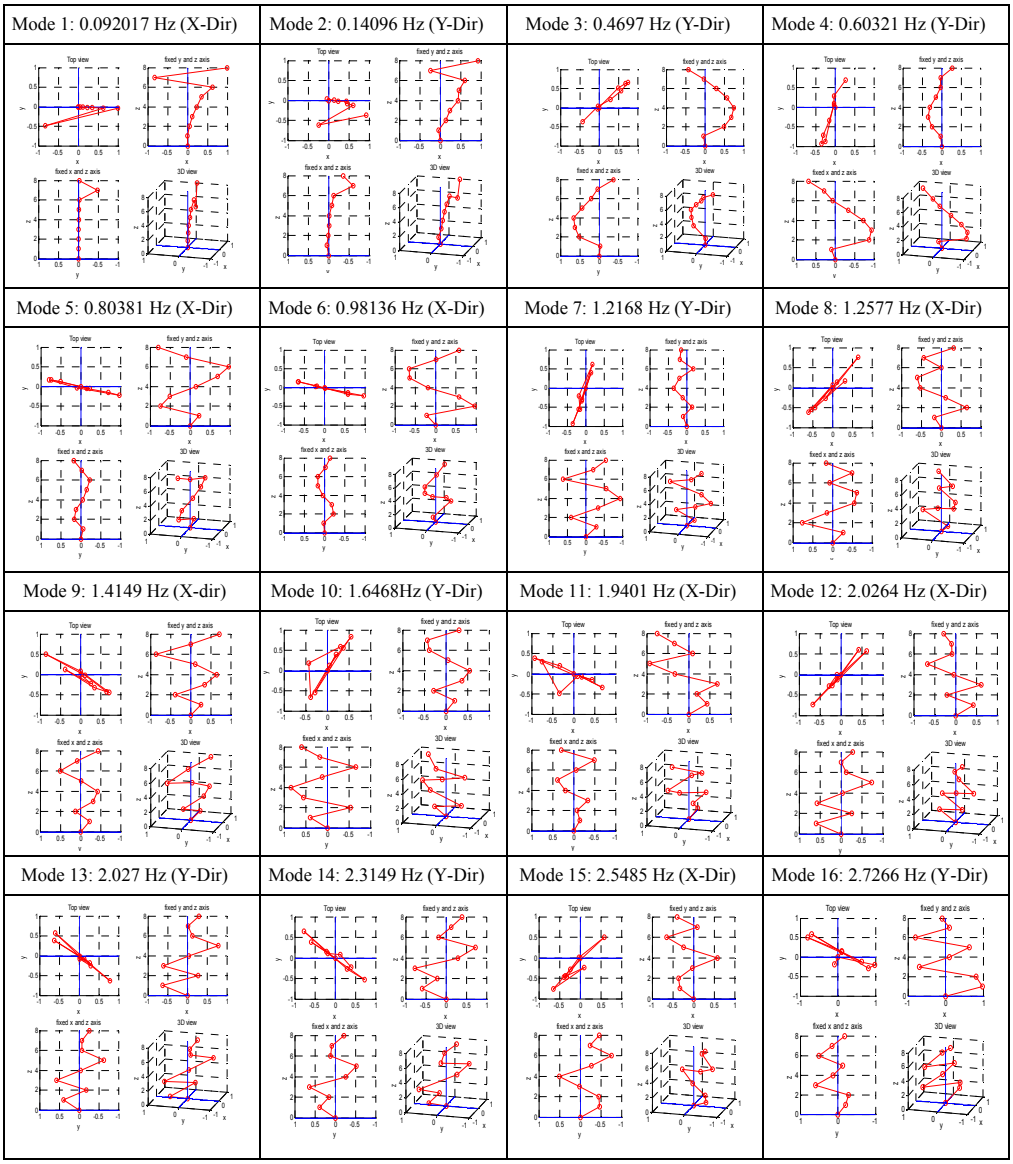

Figure 7a: Identified 16 mode shapes (top view, x- and y- direction, 3-D) from Pingtong earthquake

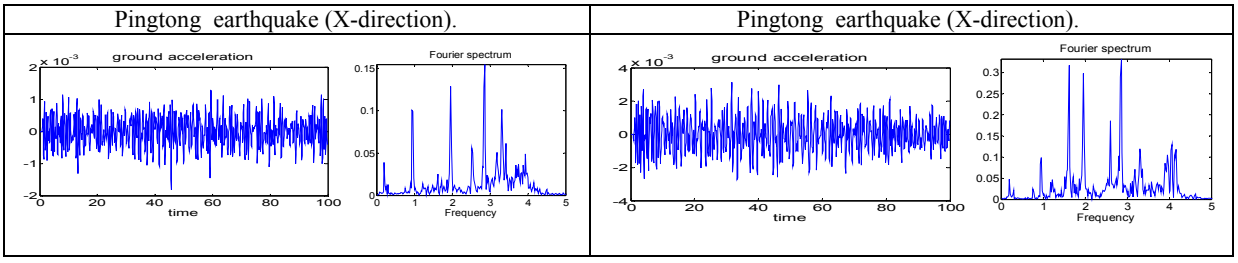

Figure 7b. Identified input forcing function on Canton tower and its Fourier amplitude (Pingtong earthquake)

CONCLUSIONS

This paper has presented the discussions on the dynamic characteristics of Canton Tower from the ambient vibration measurement as well as the earthquake response data. Four events data were selected for discussion. The dynamic characteristics of the tower before and during both Burma earthquake and Ya-An earthquake look the same. Low frequency modes can easily be identified because of the long period seismic waves generated from the far-distance earthquakes. For Heyuan earthquake, the near-site earthquake, higher frequency modes were identified during this earthquake. The summary is that for far-distance earthquake, long seismic wave can be observed which can excite

the very low frequencies of the structure (such as the high-raise Canton tower). For near-distance earthquake, high frequency ground motion signal can be observed which can excite short period of system natural frequencies. Based on the response measurements during earthquake, the input excitation force of two earthquake events at the base of the tower were identified by using input force reconstruction technique. It is observed that the identified input force for Pingtong earthquake contains higher frequency signals than the Burma earthquake. It is important to point out that for input force identification, it is assumed that the mass is uniformly distributed at each node along the tower and the mass is assumed the same, and the measurement can be taken from each degree of freedom.

ACKNOWLEDGMENTS

The authors gratefully acknowledge the support provided by the Natural Science Council of Taiwan (NSC-101-2625-M-002-015) and Excellent Research Program of The National Taiwan University (102-R891702).

REFERENCES

A Benchmark Problem on Structural Health Monitoring of High-Rise Slender Structures. Phase I: Field vibration measurement and model updating. Description of the measurement. (2009).http://www.cse.polyu.edu.hk /benchmark/ index.htm

Amani, M.G., Riera, J.D. and Curadelli, R.O. (2007). "Identification of changes in the stiffness and damping matrices of linear structures through ambient vibrations", *Structural Control and Health Monitoring*, 14, 1155-1169.

Bassville, M., Benveniste, A., Goursat, M. and Mevel, L. (2007). "In-flight vibration monitoring of aeronautical structures", *IEEE Control System Magazine*, October 2007, 27-41.

Boonyapinyo, V. and Janesupasaeree, T. (2010). "Data-driven stochastic subspace identification of flutter derivatives of bridge decks", *J. wind Eng. Ind. Aerodyn*, 98, 784-799.

Brincker, R., Zhang, L. and Andersen, P. (2000). "Modal Identification from Ambient Responses using Frequency Domain Decomposition", *Proc. of the 18th International Modal analysis Conference*, San Antonio, Texas, February 7-10.

Brincker, R., Andersen, P. and N. Møller (2000). "Output-only Modal Testing of a car body subject to Engine Excitation", *Proc. Of the 18th International Modal Analysis Conference*, San Antonio, Texas, February 7-10.

Chan, Y.T., Hu, A.G., Plant, J.B. (1979). "A Kalman filter based tracking scheme with input estimation", *IEEE Transaction of Aerospace and Electronic Systems,* Vol. AES-15, No.2, March.

Juang, J.N. and Pappa, R.S. (1956). "An eigensystem realization algorithm for modal parameter identification and model reduction", *J. Guid., Conftrol Dyn.*, 8(5), 620-627.

Liu, J.J., Ma, C.K., Kung, I.C. and Liu, D.C. (2000). "Input force estimation of a cantilever plate by using a system identification technique", *Comut. Method Appl. Mech. Engrg*. 190, 1309-1322.

Ma, C.K., Tuan, P.C. and Lin, D.C. (1998). "A study of inverse method for the estimation of impulse loads", *International of Journal of System Science,* 29 (6), pp.663-672.

Ma, C.K., Tuan, P.C., Chang, J.M., and Lin, D.C. (2003). "Adaptive weighting inverse method for the estimation of input loads", *International of Journal of System Science*, Vol. 34, No.3, pp. 181-194, February 20.

Ni, Y.Q., Xia, Y., Liao, W.Y. and Ko, J.M. (2009). "Technology innovation in developing the structural health monitoring system for Guangzhou New TV Tower", *Journal of Structural Control and Health Monitoring*, 16: 73-98.

Peeters, B. (2000). *System Identification and Damage Detection in Civil Engineering*, Ph.D. Dissertation, Katholieke Universiteit, Leuven, December.

Peeters, B. and De Roeck, G. (2001). "Stochastic system identification for operational modal analysis: a review", *J. Dyn. Syst. Meas. Control*, 123(4): 659-666.

Peeters, B. and De Roeck, G. (1999). "Refference-based stochastic subspace identification for output-only modal analysis", *Mechanical Systems and Signal Processing,* 13(6), 855-878.

Van Overschee, P. and De Moor, B. (1996). *Subspace identification for linear systems: theory – implementation – applications*, Kluwer Academic Publishers, Dordrecht, The Netherlands.

Weng, J.H., Loh, C.H., Lynch, J.P., Lu, K.C., Linn, P.Y. and Wang, Y. (2008). "Output-Only Modal Identification of a Cable-Stayed Bridge Using Wireless Monitoring Systems", *J. of Engineering Structure*, 30 (2), 1802-1830.

Wu, A.L., Loh, C.H. and Yang, J.N. (2009). "Input Force Identification: Application to Soil-Pile Interaction", J. *Structural Control & Health Monitoring*, 16, 223-240.